analytical chemistry

pubs.acs.org/ac Article

Dual 3D DNA Nanomachine-Mediated Catalytic Hairpin Assembly for Ultrasensitive Detection of MicroRNA

Xiao-Long Zhang,[§] Yang Yin,[§] Shu-Min Du, Ling-Qi Kong, Ya-Qin Chai, Zhao-Hui Li,* and Ruo Yuan*

Cite This: *Anal. Chem.* 2021, 93, 13952−13959 Read Online

ACCESS | Metrics & More | Article Recommendations | Supporting Information

ABSTRACT: Herein, we designed a dual 3D DNA nanomachine (DDNM)-mediated catalytic hairpin assembly (DDNM-CHA) to construct an electrochemical biosensor for ultrasensitive detection of miRNA, which possesses quite a faster reaction rate and much higher amplification efficiency than those of traditional catalytic hairpin assembly (CHA). Impressively, since the DDNM skillfully increases the local concentration of reactants and decreases the steric hindrance of substrates simultaneously, the DDNM-CHA could be endowed with higher collision efficiency and more effective reaction compared with traditional CHA, resulting in a hyper conversion efficiency up to 2.78×10^7 only in 25 min. This way, the developed DDNM-CHA could easily conquer the main predicaments: long reaction time and low efficiency. As a proof of the concept, we adopt the gold nanoparticles (AuNPs) and the magnetic nanoparticle (Fe_3O_4) as the kernel of DNM-A and DNM-B, respectively, and harness the magnetic electrode to directly adsorb the products H1−H2/Fe_3O_4 for constructing an immobilization-free biosensor for high-speed and ultrasensitive detection of miRNA with a detection limit of 0.14 fM. As a result, the DDNM-CHA we developed carves out a new insight to design a functional DNA nanomachine and evolve the analysis method for practical amplification in the sensing area and promotes the deeper exploration of the nucleic acid signal amplification strategy and DNA nanobiotechnology.

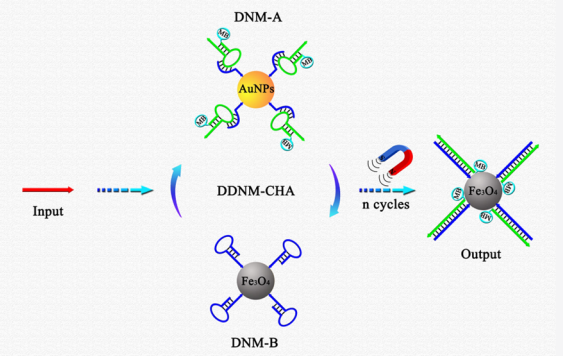

INTRODUCTION

MicroRNA (miRNA), with a short length of about only 20 ribonucleotides, plays an important role in the early diagnosis and therapy of malignant diseases since its abnormal expression levels were related to lots of human diseases.[1,2] In consequence, it is of great significance to sensitively detect miRNA with low abundance. To meet this urgent demand for accurate and sensitive identification of miRNA, several enzyme-assisted signal amplification methods like strand displacement amplification (SDA),[3,4] rolling circle amplification (RCA),[5] and loop-mediated isothermal amplification (LAMP)[6] were put forward. However, these methods suffered from low sensitivity, time consumption, and high cost,[7,8] hindering the advance of the practical applications. Alternative enzyme-free nucleic acid signal amplification methods (catalytic hairpin assembly (CHA),[9] hybridization chain reaction (HCR),[10] enzyme-free target recycling amplification (EFTRA),[11] etc.[12,13]) that rely on simpler one-step protocols were proposed, which have gained wide attention due to their simplicity and competing sensitivity. Nevertheless, these methods are also facing the problems of low conversion efficiency and long reaction time, leading to the nonspecific background leakage[14,15] and limiting their deeper exploration and wider application.

In recent years, to solve these problems mentioned above, some works based on spatial-confinement effects[16,17] or self-replication[18,19] were raised, which indeed accelerated the reaction kinetics and improved the conversion efficiency of the enzyme-free methods to some extent. Even so, the corresponding huge steric hindrance of substrates leads to less effective collision and more side reactions, resulting in relatively low reaction efficiency. Thus, increasing the local concentration of reactants for higher collision efficiency and reducing the steric hindrance of substrates for a more effective reaction simultaneously are expected to address the critical challenge of long reaction time and low efficiency in traditional enzyme-free methods.

To break these issues and inherit the advantages of these enzyme-free methods, we designed a simple and delicate dual 3D DNA nanomachine (DDNM)-mediated catalytic hairpin assembly (DDNM-CHA) by tactfully introducing extra two kernels into traditional CHA to achieve higher collision efficiency and a more effective reaction of substrates simultaneously, successfully improving the reaction rate and the conversion efficiency. First, the prepared DDNM is

Received: July 29, 2021
Accepted: September 22, 2021
Published: October 6, 2021

https://doi.org/10.1021/acs.analchem.1c03215
Anal. Chem. 2021, 93, 13952−13959

Scheme 1. Schematic Illustration of (part A) the 3D DNA Nanomachine Pair (DNMP) Consisting of DNM-A and DNM-B, (part B) DNMP-Mediated Catalytic Hairpin Assembly (DNNM-CHA), and (part C) Construction of Immobilization-free Electrochemical Biosensor for Ultrasensitive Detection of miRNA

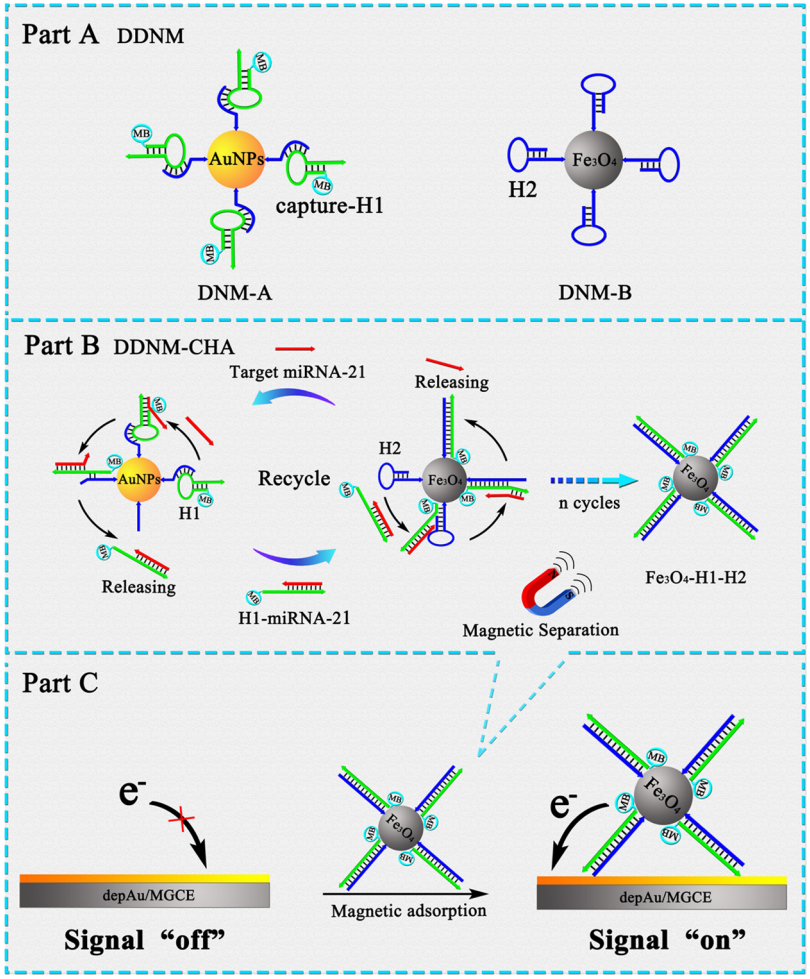

composed of 3D DNA nanomachine A (DNM-A) and 3D DNA nanomachine B (DNM-B) (Scheme 1, part A). Then, as the mechanism of DDNM-CHA shown in part B, with the target miRNA-21 as an initiator, the H1-labeled signal tag methylene blue (MB), which was concentrated on the gold nanoparticles (AuNPs) by a short DNA strand, could be opened and then removed from the AuNPs with the formation of duplex H1-miRNA. Then, the newly exposed ssDNA region within H1 could hybridize with the toehold of H2 concentrated on the Fe_3O_4 magnetic nanoparticles (Fe_3O_4 MNPs) and trigger branch migration, ultimately forming duplex H1−H2 on the MNPs and releasing the miRNA to participate in the next cycle. In this way, traces of target miRNA-21 could be converted into amounts of MB labeled on H1 to be captured on the Fe_3O_4 MNPs, which could be rapidly adsorbed on the magnetic electrode to enhance the electrochemical signal of MB by the intrinsic electrocatalytic activities,[20] cooperatively resulting in the obvious electrochemical signal response of the biosensing platform (part C). As a result, we developed a constructive signal amplification method DDNM-CHA with fast, effective, and facile properties, which gives impetus to design new nucleic acid amplification for its great potential in biosensor construction, biological nanobiotechnology, and device integration.

EXPERIMENTAL SECTION

Preparation of the Au Nanoparticles (AuNPs). According to the previous literature,[21,22] AuNPs were prepared with minor modifications. Briefly, 500 μL of $HAuCl_4$ (1%) was mixed with 100 mL of deionized ultrapure water (deionization (DI) water, ≥18.2 MΩ, Milli-Q, Millipore), and the resulting solution was heated to boiling, followed by the injection of 1.5 mL of sodium citrate (1%) under violent stirring for 15 min. Next, the mixture was cooled to room temperature and purified by centrifugation at 12 000 rpm for 30 min to remove the supernatants at least three times. Then, the obtained AuNPs were stored at less than 4 °C.

Preparation of the Complex Capture-H1 and Hairpin H2. The DNA strands H2 and the mixture of H1 and Capture in Tris-HCl buffer (pH 7.4) were, respectively, heated to 95 °C for 10 min and then cooled to room temperature over 30 min to form hairpin H2 and complex Capture-H1. The prepared hairpin DNAs were stored under 4 °C and used in subsequent experiments.

Synthesis of Complex Fe_3O_4 MNPs-H2 and AuNPs-Capture-H1. First, 300 μL of carboxyl-modified Fe_3O_4 MNPs were washed with distilled water three times. Next, the washed Fe_3O_4 MNPs were dissolved in 400 μL of Tris-HCl buffer solution (pH 7.4) containing EDC (20 mM) and then stirred for 20 min at 4 °C to activate the carboxyl group. Subsequently, the

https://doi.org/10.1021/acs.analchem.1c03215
Anal. Chem. 2021, 93, 13952−13959

Fe_3O_4 MNPs-H2 was prepared as follows: 50 μL of H2 modified with amino (4 μM), 5 μL of NHS (200 mM), and 50 μL of the treated Fe_3O_4 MNP solution were mixed and agitated for 5 h at 4 °C.

The AuNPs-Capture-H1 was formed as follows: The amino-modified Capture- H1 was mixed with the prepared AuNPs by sonicating for 15 min and then shaking at 4 °C for 5 h, resulting in the attachment of H1-Capture onto the surface of AuNPs by a Au−N bond, followed by centrifugation at 12 000 rpm for 15 min. Finally, the solutions of AuNPs-Capture-H1 and Fe_3O_4 MNPs-H2 were, respectively, stored in Tris-HCl (pH 7.4) buffer at 4 °C for subsequent use.

Process of the Modified Electrode Preparation. First, a bare magnetic glassy carbon electrode (MGCE, 4 mm in diameter) was polished carefully with an alumina slurry (0.3 and 0.05 μm), followed by ultrasonic treatment with ethanol and deionized ultrapure water. Subsequently, the electrode was immersed into a $HAuCl_4$ aqueous solution (1%) and electrodeposited at −0.2 V for 30 s to coat a layer of gold particles (depAu).

Subsequently, 10 μL of the reacted solution was incubated onto the electrode surface (depAu/MGCE) for 1 min to magnetically adsorb the Fe_3O_4 MNPs at room temperature. Then, the electrode was rinsed with Tris-HCl buffer gently to remove the reacted solution.

Dual 3D DNA Nanomachine-Mediated Catalytic Hairpin Assembly (DDNM-CHA). First, the initiator miRNA-21 was mixed with the prepared DNM-A (AuNPs-Capture-H1) and DNM-B (Fe_3O_4 MNPs-H2) in Tris-HCl buffer and reacted together. After the reaction was finished, the mixture was purified through magnetic separation and rinsed with Tris-HCl buffer three times. Then, 10 μL of the above-obtained mixture was dropped on the electrode (depAu/MGCE) and incubated under the optimal conditions. Finally, the electrode was washed with Tris-HCl buffer (pH 7.4) for subsequent electrochemical measurements.

RESULTS AND DISCUSSION

Characterization of the Nucleic Acid Reaction. The reaction mechanism of the nucleic acid was characterized by PAGE. As displayed in Figure 1, the bright bands in lanes 1−5 represent target miRNA-21, Capture, hairpin H1, hairpin H2, and duplex Capture-H1, respectively. After the miRNA-21 was mixed with hairpin H1 (lane 6), in comparison with lane 1 and lane 3, a new band with slower migration (duplex H1-miRNA-21) could be observed and the band corresponding to miRNA-21 almost vanished, suggesting that hairpin H1 was opened and hybridized with the target miRNA-21. While the miRNA-21 was mixed with duplex Capture-H1 (lane 7), a band representing duplex H1-miRNA-21 like the one in lane 6 and a band corresponding to Capture appeared simultaneously, which verified that H1 can also be opened by miRNA after being connected to Capture DNA. Then, after H2 was added into the mixture of miRNA-21 and H1, a new obvious band with slower migration (lane 8) than that of duplex H1-miRNA-21 could be noticed, indicating that H2 successfully hybridized with duplex H1-miRNA-21 and displaced miRNA-21. These abovementioned observations strongly indicated that the input of target miRNA-21 could successfully trigger DNNM-CHA, accompanied by enormous output duplex H1−H2.

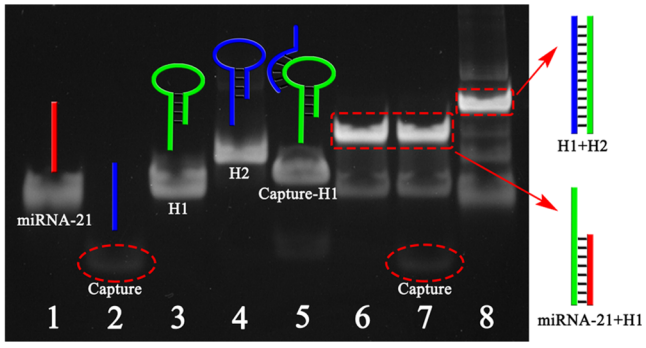

Figure 1. Nondenaturing PAGE characterization of the nucleic acid reaction: lane 1, miRNA-21 (4 μM); lane 2, Capture (4 μM); lane 3, H1 (2 μM); lane 4, H2 (2 μM); lane 5, Capture-H1 (2 μM); lane 6, miRNA-21 (2 μM) + H1 (2 μM); lane 7, miRNA-21 (2 μM) + Capture-H1 (2 μM); and lane 8, miRNA-21 (2 μM) + H1 (2 μM) + H2 (2 μM) (PAGE 16%, 60 mA, 40 min).

Performance Comparison of DDNM-CHA with Other CHA Systems. First, transmission electron microscopy (TEM) (Figure S1), UV−vis absorption spectra (Figure S2), and ζ-potential measurements (Figure S3) were adopted to characterize the successful formation of AuNPs, AuNPs-Capture-H1, Fe_3O_4 MNPs, and Fe_3O_4 MNPs-H2. Subsequently, to verify the performance of the proposed DNNM-CHA, some different CHA systems in Figure 2A (a, wild CHA; b, 3D DNA nanomachine-assisted CHA-1 (DNM-CHA-1); c, 3D DNA nanomachine-assisted CHA-2 (DNM-CHA-2)) were set as control groups, and real-time fluorescence was employed to monitor the dynamic status of these reactions. Based on fluorophore FAM and quencher BHQ1, which were labeled on DNA strands (Table S1), this way, a fluorescence intensity decrease was measured as duplex H1−H2 was formed. As shown in Figure 2B, after the introduction of miRNA-21, the fluorescence intensity of DNNM-CHA (curve d) decreased much faster to a lower value compared with those of wild CHA (curve a), DNM-CHA-1 (curve b), and DNM-CHA-2 (curve c), indicating the dramatically evolved thermodynamical and dynamical performance of DNNM-CHA.

To obtain the specific data comparison of the thermodynamical and dynamical performance of these methods, the fluorescence intensity was taken as the derivative of the time, and the results in Figure 2C displayed that the initial reaction rate of DNNM-CHA in fluorescence (-41.79 au s^{-1}) is obviously faster than those of DNM-CHA-1 (-10.18 au s^{-1}), DNM-CHA-2 (-24.52 au s^{-1}), and wild CHA (-7.09 au s^{-1}). While the change of the fluorescence intensity approached 0, the DNNM-CHA reached a balance with the corresponding reaction time of 1550 s (CHA: 4216 s, DNM-CHA-1: 4216 s, DNM-CHA-2: 4000 s). Based on the relationship of fluorescence intensity with the concentration of fluorophore FAM, as shown in Figure 2D, the calculated average reaction rate (the ratio between the concentration of the resultant and the balanced reaction time) of DNNM-CHA (6.02×10^{-10} M s^{-1}) is about 4 times that of wild CHA (1.62×10^{-10} M s^{-1}) and is also larger than those of DNM-CHA-1 (1.81×10^{-10} M s^{-1}) and DNM-CHA-2 (2.14×10^{-10} M s^{-1}) (the concentration of duplex H1−H2 was calculated based on Figure 2D). Furthermore, we also obtained the kinetic constant k of these methods by building the corresponding model. Since the kinetics of a toehold strand displacement reaction (TSDR)[23] at a sufficiently low concentration are well approximated by bimolecular reactions with second-order rate constants,[24] assuming the reactants quickly resolve into products,[25] the

https://doi.org/10.1021/acs.analchem.1c03215
Anal. Chem. 2021, 93, 13952−13959

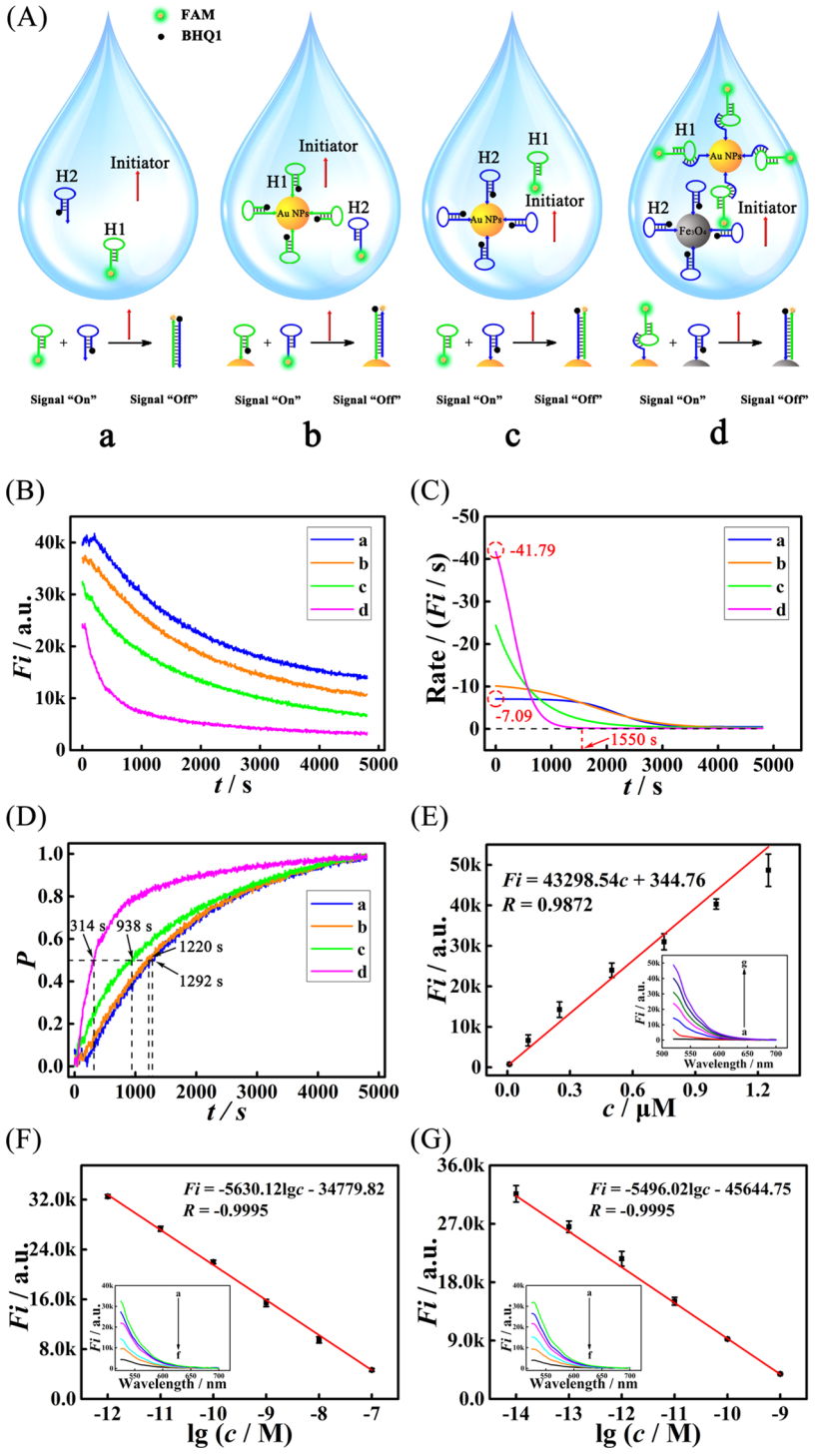

Figure 2. (A) Raw reactants and the schematic diagram of fluorescence label analysis; (B) kinetic experiments; (C) reaction rates of the wild CHA (a), DNM-CHA-1 (b), DNM-CHA-2 (c), and DNNM-CHA (d) in the presence of 1 nM initiator miRNA-21 (the concentration of H1 and H2 was 1 μM); (D) cumulative probability converted by fluorescence signal over time measured for (a) wild CHA, (b) DNM-CHA-1, (c) DNM-CHA-2, and (d) DNNM-CHA in the presence of 1 nM initiator miRNA-21 (the concentration of H1 and H2 was 1 μM); (E) calibration plot for the fluorescence intensity vs c (the inset with fluorescence intensities to different concentrations of the fluorophore FAM: (a) 0.01 μM, (b) 0.1 μM, (c) 0.25 μM, (d) 0.5 μM, (e) 0.75 μM, (f) 1.0 μM, and (g) 1.25 μM); (F) calibration plot for the fluorescence intensity vs initiator miRNA-21 concentrations (the inset with fluorescence intensities in wild CHA to different concentrations of the initiator miRNA-21: (a) 1 pM, (b) 10 pM, (c) 100 pM, (d) 1 nM, (e) 10 nM, and (f) 100 nM); and (G) galibration plot for the fluorescence intensity vs initiator miRNA-21 concentrations (the inset with fluorescence intensities in DNNM-CHA to different concentrations of the initiator miRNA-21: (a) 10 fM, (b) 100 fM, (c) 1 pM, (d) 10 pM, (e) 100 pM, and (f) 1 nM) (error bars, SD, n = 3).

reaction process of these CHA systems, which are developed based on TSDR could be modeled as

$$\mathrm{H1} + \mathrm{H2} \xrightarrow[k]{\mathrm{miRNA}} \mathrm{H1H2} \quad (1)$$

https://doi.org/10.1021/acs.analchem.1c03215
Anal. Chem. 2021, 93, 13952−13959

where k represents the second-order rate constant. According to the related kinetic study,[26,27] k could be computed by the equation

$$t_{1/2} = \frac{1}{kc_0} \quad (2)$$

where $t_{1/2}$ represents half-period and c_0 is the initial concentration of reactants. Especially, after converting the fluorescence intensity into P (the cumulative probability (P)) represents the degree of conversion calculated by dividing the number of satellite leaving events up to a given time by the total number of events observed during the experimental time course, as shown by results in Figure 4D, $t_{1/2}$ values of DNNM-CHA and CHA were 314 and 1292 s, respectively. Then, based on eq 2, some kinetic parameters can be estimated, respectively, as shown in Table 1. Especially, the obtained rate constant k of

Table 1. Comparison of the Developed DNNM-CHA with Other CHA Systems (with 1 nM miRNA-21)

CHA systems	initial rate in fluorescence (au s^{-1})	average rate ($M\ s^{-1}$)	kinetic constant k ($M^{-1}\ s^{-1}$)
CHA	−7.09	1.62×10^{-10}	7.74×10^{2}
M-CHA-1	−10.18	1.81×10^{-10}	8.20×10^{2}
M-CHA-2	−24.52	2.14×10^{-10}	1.07×10^{3}
DNNM-CHA	−41.79	6.02×10^{-10}	3.18×10^{3}

DNNM-CHA ($k_{DNNM\text{-}CHA} = 3.85 \times 10^3\ M^{-1}\ s^{-1}$) was almost 5 times that of wild CHA ($k_{CHA} = 7.74 \times 10^2\ M^{-1}\ s^{-1}$), showing the quite more excellent kinetic performance of DNNM-CHA.

Otherwise, to obtain the conversion efficiency of wild CHA and DNNM-CHA, the relationship between the fluorescence intensity and the initiator miRNA-21 concentration was studied, and the results are shown in Figure 2F,G. With the increased concentration of miRNA-21, the fluorescence intensity of these two systems decreased, and the corresponding regression equations for the fluorescence intensity vs c were Fi = −34779.82−5630.12 lg c (from 1 pM to 100 nM ($1 \times 10^{-13}\ M^{-1} \times 10^{-7}$ M), $R = -0.9995$) and Fi = −45644.75−5496.02 lg c (from 10 fM to 1 nM ($1 \times 10^{-14}\ M^{-1} \times 10^{-9}$ M), $R = -0.9995$), respectively (Fi and c represent the fluorescence intensity and the miRNA concentration, respectively; unit of c is M). Then, based on Figure 2E, the specific conversion efficiency (N) with different initiator miRNA-21 concentrations was calculated out (Table S2), in which the maximum N of DNNM-CHA ($N_{DNNM\text{-}CHA}$: 9.19×10^2−2.78×10^7) was more than two orders of magnitude beyond those of CHA (N_{CHA}: 9.00×10^0−2.57×10^5), respectively, illustrating the extraordinary amplification performance of DNNM-CHA. These above-mentioned results demonstrated that the developed DNNM-CHA indeed achieved a lot of strides either in the dramatically improved reaction rate or conversion efficiency when compared with CHA, which was ascribed to the fact that the introduction of the two kernels in CHA could obviously improve the collision probability and decrease the steric hindrance, promoting the proceeding of the whole hybridization reaction.

Subsequently, DNNM-CHA was applied to construct a biosensing platform for the ultrasensitive detection of miRNA-21. First, the stepwise fabrication of the biosensor based on DNNM-CHA was successfully verified by cyclic voltammetry (CV) and electrochemical impedance spectroscopy (EIS) (Figures S4 and S5). Then, the feasibility of the proposed biosensing platform for miRNA-21 detection was certified by square wave voltammetry (SWV) (Figure S6).

Response of the Proposed Biosensor Based on DNNM-CHA for miRNA Detection. As a proof of concept, DNNM-CHA was used as a high-efficiency DNA signal magnifier to construct a biosensor for the rapid and ultrasensitive detection of miRNA. Under the optimal experimental conditions (Figure S7), the proposed biosensor was incubated with different concentrations of target miRNA-21 and monitored by SWV. As shown in Figure 3A, the SWV current response increased gradually as the target concentration elevated from 0.2 fM to 1 nM and displayed a well linear relationship with the logarithm of the miRNA-21 concentration. As shown in Figure 3B, the regression equation is expressed as $I = 3.1679 + 0.1969$ lg c with a correlation-coefficient value (R) of 0.9969. According to the 3σ rule, a detection limit of 0.139 fM miRNA-21 was calculated out (Supporting Information, page S15 and S16). Compared with other biosensing platforms, as illustrated in Table 2, the

Table 2. Comparison of the Biosensor Developed by DNNM-CHA with Other miRNA Detection Methods

analytical methods	linear range	detection limit	refs
fluorescence	100 pM−50 nM	85.3 pM	28
photoacoustic Imaging	10 pM−100 nM	11.69 pM	29
electrochemiluminescence	10 fM−0.1 nM	6.6 fM	30
photoelectrochemical	1 fM−10 pM	0.5 fM	31
electrochemical	0.14−10 nM	40 pM	32
electrochemical	10 fM−20 nM	10 fM	33
electrochemical	0.2 fM−1 nM	0.139 fM	this work

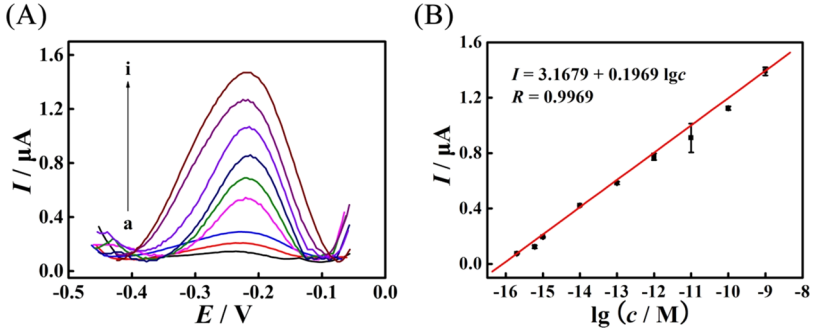

Figure 3. (A) SWV current responses of the biosensors to different concentrations of the target miRNA-21: (a) 0.2 fM, (b) 0.6 fM, (c) 1.0 fM, (d) 10 fM, (e) 100 fM, (f) 1.0 pM, (g) 10 pM, (h) 100 pM, and (i) 1 nM. (B) Corresponding calibration plot for the SWV peak current vs lg c (error bars, SD, n = 3).

https://doi.org/10.1021/acs.analchem.1c03215
Anal. Chem. 2021, 93, 13952−13959

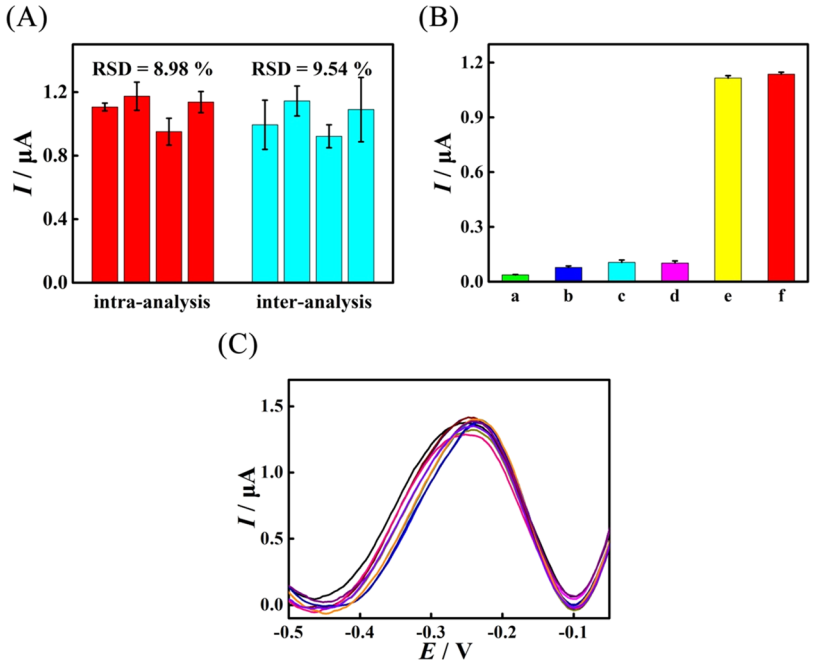

Figure 4. (A) Reproducibility (100 pM miRNA-21) of the biosensensing platform; (B) selectivity of the electrochemical biosensor: (a) blank sample, (b) miRNA-126 (10 nM), (c) miRNA-141 (10 nM), (d) miRNA-155 (10 nM), (e) miRNA-182-5P (10 nM), (f) miRNA-21 (100 pM), and (g) mixed sample; and (C) stability of the elaborated biosensor (100 pM miRNA-21) (error bars, SD, n = 3).

prepared biosensor had an attractively wider linear range and an extremely lower detection limit that could be ascribed to the elaborated DNNM-CHA with hyper conversion efficiency.

Reproducibility, Selectivity, and Stability of the Biosensor. To further study the performance of these proposed biosensors comprehensively, the reproducibility, selectivity, and stability of the biosensing platform were validated. To confirm the reproducibility of the biosensing platform, the necessary index for real biomarker detection, four prepared biosensors with 100 pM miRNA-21 were studied under the same determination condition. As displayed in Figure 4A, a relative standard deviation (RSD) of 8.98% was achieved. Moreover, a set of electrodes with the same miRNA-21 (100 pM) were detected after 5 days, and the RSD was 9.54%. The remarkable results indicate that the combination of the evolved C-CHA for biomarker detection presented an acceptable reproducibility.

To assess the selectivity of this biosensor, five interference agents including miRNA-126, miRNA-141, miRNA-155, and miRNA-182-5P were evaluated under the same experimental condition. As shown in Figure 4B, the obvious current response of the electrode could be observed only with miRNA-21 (100 pM, f). Oppositely, in the presence of the interference agents including miRNA-126 (10 nM, b), miRNA-141 (10 nM, c), miRNA-155 (10 nM, d), and miRNA-182-5p (10 nM, e), the current responses were negligible. In addition, the mixed analytical solution containing 100 pM target miRNA-21 was also analyzed with the biosensing system, exhibiting an obvious current response as expected (g). These abovementioned results demonstrated high selectivity of the biosensor.

The stability, which was critical to its practical application, especially in a complicated biomedical environment, was evaluated by successive scans of the sensing platform with detection of 100 pM miRNA-21 100 times. As displayed in Figure 4C, when compared with the initial electrochemical response, the SWV current intensity only changed from 93.6 to 103.0% with the RSD = 2.79%, indicating desirable stability of our biosensing surface.

Real Application of the Biosensing Platform in Cancer Cells. The total RNA lysate solutions from the human cancer-cell lines (MCF-7 and HeLa) were employed to study the capacity of the developed biosensing platform for the determination of miRNA-21 in real biological samples. As depicted in Figure 5, the SWV signal response gradually

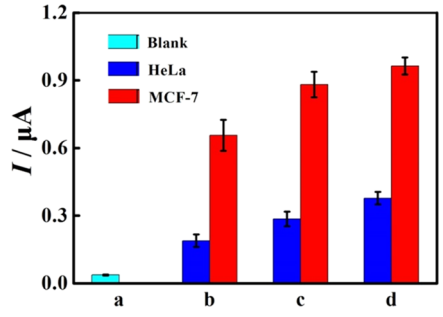

Figure 5. Current response of the developed biosensor from different cancer-cell lysates: (a) Blank sample, (b) HeLa (100 cells) and MCF-7 (100 cells), (c) HeLa (1000 cells) and MCF-7 (1000 cells), and (d) HeLa (10 000 cells) and MCF-7 (10 000 cells) (the cell lysates incubated on the electrode were obtained from such cancer cells with the corresponding number; error bars, SD, n = 3).

increased with the increased cell numbers, instructing an obvious expression level of miRNA-21 in MCF-7, whereas no obvious SWV responses were observed in blank samples and HeLa cells, indicating a low expression level compared to that of MCF-7. The abovementioned results were consistent with previous research,[34,35] further demonstrating that this quantification of miRNA-21 in cancer cells possesses the key potential for clinical diagnosis of cancers.

https://doi.org/10.1021/acs.analchem.1c03215
Anal. Chem. 2021, 93, 13952−13959

CONCLUSIONS

In summary, unlike the traditional nucleic acid signal amplification methods, the dikernel-assisted catalytic hairpin assembly (DNNM-CHA) we proposed realizes the improved collision probability and the decreased steric hindrance by introducing AuNPs and Fe_3O_4 MNPs as two kernels, which promotes the proceeding of the whole hybridization reaction, therefore achieving a high reaction speed and hyper conversion efficiency compared with those of traditional catalytic hairpin assembly (CHA). Benefiting from these advantages, the DNNM-CHA is successfully applied as a high-efficiency DNA signal amplifier to construct an immobilization-free biosensor for the rapid and ultrasensitive detection of miRNA-21, which carves out a span-new way to design a potential strategy for the biosensing assay and clinic diagnosis. Otherwise, the DNNM-CHA also proposes a creative insight to explore the inherent property of nucleic acid amplification for advancing its superiority and applicability in diagnostic applications, biological research, nanobiotechnology, and so on.

ASSOCIATED CONTENT

Supporting Information

The Supporting Information is available free of charge at https://pubs.acs.org/doi/10.1021/acs.analchem.1c03215.

Experimental Section; mechanism illustration of the cross-linking process between the carboxyl-modified Fe_3O_4 and H2 modified with amino; characterization of AuNPs, AuNPs-Capture-H1, Fe_3O_4 MNPs, and Fe_3O_4 MNPs-H2; experimental conversion efficiency N of DNNM-CHA and CHA with different concentrations of the initiator by fluorescence; electrochemical characterization of the designed biosensing platform; feasibility of the proposed biosensing platform for miRNA-21 detection; optimization of the experimental conditions of DNNM-CHA; and the limit of detection calculation for the miRNA biosensing (PDF)

AUTHOR INFORMATION

Corresponding Authors

Zhao-Hui Li − *Henan Joint International Research Laboratory of Green Construction of Functional Molecules and Their Bioanalytical Applications, College of Chemistry, Zhengzhou University, Zhengzhou 450001, P. R. China;* orcid.org/0000-0003-3946-0656; Email: zhaohui.li@zzu.edu.cn

Ruo Yuan − *Key Laboratory of Luminescence Analysis and Molecular Sensing (Southwest University), Ministry of Education, College of Chemistry and Chemical Engineering, Southwest University, Chongqing 400715, P. R. China;* orcid.org/0000-0003-3664-6236; Email: yuanruo@swu.edu.cn; Fax: +86 2368253172

Authors

Xiao-Long Zhang − *Key Laboratory of Luminescence Analysis and Molecular Sensing (Southwest University), Ministry of Education, College of Chemistry and Chemical Engineering, Southwest University, Chongqing 400715, P. R. China*

Yang Yin − *Key Laboratory of Luminescence Analysis and Molecular Sensing (Southwest University), Ministry of Education, College of Chemistry and Chemical Engineering, Southwest University, Chongqing 400715, P. R. China*

Shu-Min Du − *Key Laboratory of Luminescence Analysis and Molecular Sensing (Southwest University), Ministry of Education, College of Chemistry and Chemical Engineering, Southwest University, Chongqing 400715, P. R. China*

Ling-Qi Kong − *Key Laboratory of Luminescence Analysis and Molecular Sensing (Southwest University), Ministry of Education, College of Chemistry and Chemical Engineering, Southwest University, Chongqing 400715, P. R. China*

Ya-Qin Chai − *Key Laboratory of Luminescence Analysis and Molecular Sensing (Southwest University), Ministry of Education, College of Chemistry and Chemical Engineering, Southwest University, Chongqing 400715, P. R. China;* orcid.org/0000-0003-4392-9592

Complete contact information is available at: https://pubs.acs.org/10.1021/acs.analchem.1c03215

Author Contributions

[§]X.-L.Z. and Y.Y. contributed equally to this work.

Notes

The authors declare no competing financial interest.

ACKNOWLEDGMENTS

This work was financially supported by the National Natural Science Foundation of China (21974108, 21775124, and 21675129) and the Fundamental Research Funds for the Central Universities (XDJK2019TJ002), China.

REFERENCES

(1) Ambros, V. *Nature* **2004**, *431*, 350−355.
(2) Boon, R. A.; Iekushi, K.; Lechner, S.; Seeger, T.; Fischer, A.; Heydt, S.; Kaluza, D.; Treguer, K.; Carmona, G.; Bonauer, A.; Horrevoets, A. J.; Didier, N.; Girmatsion, Z.; Biliczki, P.; Ehrlich, J. R.; Katus, H. A.; Muller, O. J.; Potente, M.; Zeiher, A. M.; Hermeking, H.; Dimmeler, S. *Nature* **2013**, *495*, 107−110.
(3) Koc, K. N.; Stodola, J. L.; Burgers, P. M.; Galletto, R. *Nucleic Acids Res.* **2015**, *43*, 4179−4190.
(4) Zhou, W. H.; Hu, L.; Ying, L. M.; Zhao, Z.; Chu, P. K.; Yu, X. F. *Nat. Commun.* **2018**, *9*, No. 5012.
(5) Wang, J.; Wang, H. M.; Wang, H.; He, S. Z.; Li, R. M.; Deng, Z.; Liu, X. Q.; Wang, F. A. *ACS Nano* **2019**, *13*, 5852−5863.
(6) Tang, Z. F.; Choi, G.; Nouri, R.; Guan, W. H. *Nano Lett.* **2019**, *19*, 7927−7934.
(7) Yin, B. C.; Liu, Y. Q.; Ye, B. C. *J. Am. Chem. Soc.* **2012**, *134*, 5064−5067.
(8) Yuan, H.; Chao, Y. C.; Shum, H. C. *Small* **2020**, *16*, No. 1904469.
(9) Zhou, Z. X.; Brennan, J. D.; Li, Y. F. *Angew. Chem., Int. Ed.* **2020**, *59*, 10401−10405.
(10) Prinzen, A. L.; Saliba, D.; Hennecker, C.; Trinh, T.; Mittermaier, A.; Sleiman, H. F. *Angew. Chem., Int. Ed.* **2020**, *59*, 12900−12908.
(11) Hu, J. M.; Sheng, Y.; Kwak, K. J.; Shi, J. F.; Yu, B. H.; Lee, L. J. *Nat. Commun.* **2017**, *8*, No. 1683.
(12) Wu, C. C.; Cansiz, S.; Zhang, L. Q.; Teng, I. T.; Qiu, L. P.; Li, J.; Liu, Y.; Zhou, C. S.; Hu, R.; Zhang, T.; Cui, C.; Cui, L.; Tan, W. H. *J. Am. Chem. Soc.* **2015**, *137*, 4900−4903.
(13) Srinivas, N.; Parkin, J.; Seelig, G.; Winfree, E.; Soloveichik, D. *Science* **2017**, *358*, No. eaal2052.
(14) Karunanayake Mudiyanselage, A. P. K. K.; Yu, Q. K.; Leon-Duque, M. A.; Zhao, B.; Wu, R.; You, M. X. *J. Am. Chem. Soc.* **2018**, *140*, 8739−8745.
(15) Arter, W. E.; Yusim, Y.; Peter, Q.; Taylor, C. G.; Klenerman, D.; Keyser, U. F.; Knowles, T. P. J. *ACS Nano* **2020**, *14*, 5763−5771.
(16) Jung, C.; Allen, P. B.; Ellington, A. D. *Nat. Nanotechnol.* **2016**, *11*, 157−163.
(17) Cheng, H.; Li, W.; Duan, S. D.; Peng, J. X.; Liu, J. Q.; Ma, W. J.; Wang, H. Z.; He, X. X.; Wang, K. M. *Anal. Chem.* **2019**, *91*, 10672−10678.
(18) Yue, S. Z.; Song, X. Y.; Song, W. L.; Bi, S. *Chem. Sci.* **2019**, *10*, 1651−1658.

(19) Zhu, Z.; Duan, X.; Li, Q.; Wu, R.; Wang, Y.; Li, B. *J. Am. Chem. Soc.* **2020**, *142*, 4481−4492.
(20) Zheng, T. T.; Zhang, Q. F.; Feng, S.; Zhu, J. J.; Wang, Q.; Wang, H. *J. Am. Chem. Soc.* **2014**, *136*, 2288−2291.
(21) Dutta Chowdhury, A.; Agnihotri, N.; Doong, R.; De, A. *Anal. Chem.* **2017**, *89*, 12244−12251.
(22) Liang, H.; Kundu, S. *Adv. Mater.* **2008**, *20*, 826−831.
(23) Yang, X. L.; Tang, Y. N.; Traynor, S. M.; Li, F. *J. Am. Chem. Soc.* **2016**, *138*, 14076−14082.
(24) Zhang, D.; Winfree, E. *J. Am. Chem. Soc.* **2009**, *131*, 17303−17314.
(25) Song, T.; Xiao, S.; Yao, D.; Huang, F.; Hu, M.; Liang, H. *Adv. Mater.* **2014**, *26*, 6181−6185.
(26) Umezawa, K.; Yoshida, M.; Kamiya, M.; Yamasoba, T.; Urano, Y. *Nat. Chem.* **2017**, *9*, 279−286.
(27) Figg, C. A.; Winegar, P. H.; Hayes, O. G.; Mirkin, C. A. *J. Am. Chem. Soc.* **2020**, *142*, 8596−8601.
(28) Yang, F.; Cheng, Y.; Cao, Y.; Zhang, Y.; Dong, H.; Lu, H.; Zhang, X. *Anal. Chem.* **2019**, *91*, 9828−9835.
(29) Zhang, K.; Meng, X.; Yang, Z.; Cao, Y.; Cheng, Y.; Wang, D.; Lu, H.; Shi, Z.; Dong, H.; Zhang, X. *Adv. Mater.* **2019**, *31*, No. 1807888.
(30) Zhang, P.; Jiang, J.; Yuan, R.; Zhuo, Y.; Chai, Y. Q. *J. Am. Chem. Soc.* **2018**, *140*, 9361−9364.
(31) Zhang, N.; Shi, X. M.; Guo, H. Q.; Zhao, X.-Z.; Zhao, W.-W.; Xu, J. J.; Chen, H. Y. *Anal. Chem.* **2018**, *90*, 11892−11898.
(32) Castañeda, A. D.; Brenes, N. J.; Kondajji, A.; Crooks, R. M. *J. Am. Chem. Soc.* **2017**, *139*, 7657−7664.
(33) Mensah, K.; Cissé, I.; Pierret, A.; Rosticher, M.; Palomo, J.; Morfin, P.; Plaçais, B.; Bockelmann, U. *Adv. Healthcare Mater* **2020**, *9*, No. 2000260.
(34) Wang, Z.; Han, J.; Cui, Y.; Zhou, X.; Fan, K. *Biochem. Biophys. Res. Commun.* **2013**, *439*, 384−389.
(35) Li, S.; Xu, L.; Ma, W.; Wu, X.; Sun, M.; Kuang, H.; Wang, L.; Kotov, N. A.; Xu, C. *J. Am. Chem. Soc.* **2016**, *138*, 306−312.

https://doi.org/10.1021/acs.analchem.1c03215
Anal. Chem. 2021, 93, 13952−13959